Frontiers in Bioscience Landmark

Front. Biosci. (Landmark Ed) **2025**; 30(3): 27954
https://doi.org/10.31083/FBL27954

Original Research

Growth Arrest-specific 1 Inhibits Keap1/Nrf2 Signaling Transduction in the Activation of the Ferroptosis Program in Retinal Müller Cells

Rongfeng Dai[1], Yu Qian[1], Siqi Liu[1], Xi Zou[2], Shanshan Sun[2], Zhuo Sun[2,*]

[1]Department of Endocrinology, the Third People's Hospital of Changzhou, 213001 Changzhou, Jiangsu, China
[2]Department of Ophthalmology, the Third People's Hospital of Changzhou, 213001 Changzhou, Jiangsu, China
*Correspondence: Ssunzhuo_sz@163.com (Zhuo Sun)

Academic Editor: Sung Eun Kim
Submitted: 7 November 2024 Revised: 25 December 2024 Accepted: 2 January 2025 Published: 18 March 2025

Abstract

Background: Diabetes retinopathy (DR) represents a microvascular disease in diabetes. Growth arrest-specific 1 (GAS1) is differentially expressed in rat retinal Müller cells under high glucose (HG) conditions, and its promotion of ferroptosis contributes to retinal cell death. However, the influence of GAS1 in DR is elusive. Herein, we aimed to investigate the effect and potential mechanism based on GAS1-mediated ferroptosis on DR. **Methods**: After HG treatment, the differentially expressed genes in rat retinal Müller cells were analyzed by transcriptome sequencing followed by Kyoto Encyclopedia of Genes and Genomes (KEGG) and Gene Ontology (GO) analyses; finally, GAS1 was selected. The effects of GAS1 knockdown/overexpression and nuclear factor erythroid 2-related factor (Nrf2) silencing on viability, apoptosis, lipid peroxidation, Fe^{2+}, and oxidative stress levels in HG-induced/transfected Müller cells were measured by Cell Counting Kit-8 (CCK-8) assay, flow cytometry, and commercial reagent kits. The potential effects of GAS1 and Nrf2, especially on GAS1, Nrf2, and Kelch-like ECH-associated protein 1 (Keap1) expressions in cells, were determined by quantitative real-time polymerase chain reaction (qRT-PCR) or Western blot. **Results**: HG treatment decreased cell viability and glutathione (GSH) levels and increased apoptosis, lipid reactive oxygen species (ROS), glutathione disulfide (GSSG), malondialdehyde (MDA), oxidative stress, and Fe^{2+} levels in Müller cells ($p < 0.01$). HG treatment also upregulated GAS1, Keap1, and total Nrf2 expressions while downregulating nuclear Nrf2 in Müller cells ($p < 0.001$). GAS1 downregulation enhanced cell viability, GSH levels, and nuclear Nrf2 expression while reducing the levels of apoptosis, lipid ROS, GSSG, MDA, Fe^{2+}, Keap1, and total Nrf2 in HG-treated Müller cells ($p < 0.001$), whereas GAS1 overexpression had the opposite effects. Additionally, Nrf2 silencing reversed the impact of GAS1 overexpression in HG-treated Müller cells ($p < 0.05$). **Conclusion**: GAS1 inhibits Keap1/Nrf2 signaling transduction in activating ferroptosis in retinal Müller cells; thus, this study can aid in setting the stage for novel treatment methods against DR.

Keywords: diabetes retinopathy; GAS1; Keap1/Nrf2; ferroptosis; Müller cells

1. Introduction

Diabetes retinopathy (DR), a vision-impairing ocular disease, stands as a leading contributor of blindness in diabetes patients [1,2]. The onset of DR is attributed to chronic hyperglycemia that inflicts damage on the retinal capillaries, hindering light perception and signal transmission [1]. Working-age population constitutes the most sufferers of DR, with projections estimating 191 million DR cases by 2023 [3]. Notwithstanding the improvements in new treatment and metabolic control of diabetes patients, effective early screening and diagnostic techniques are still urgently needed [4–6]. Therefore, in-depth research on the pathogenesis of DR and exploration of potential biomarkers is of great significance to preventing, screening, and treating DR.

Ferroptosis, a newly characterized form of cell death under induction of iron-dependent lipid peroxidation, is distinguished from other forms of cell death, incorporating necrosis, pyroptosis, apoptosis, and autophagy [7,8]. Ferroptosis has demonstrated effects on the pathophysiology and pathogenesis of diabetes and its complications containing DR [9]. Ferroptosis inhibitor prevents the early DR and sustains normal visual function [10], and repressing ferroptosis mitigates the lipid peroxidation and oxidative stress injury of DR [11], implying the potential of targeting ferroptosis in treating DR. Growth arrest-specific 1 (GAS1), a multifunctional protein initially pertinent to cell cycle arrest, is also an active regulator of cell proliferation during development [12]. GAS1 induces cell death by an intrinsic apoptotic pathway [13]. Besides, *GAS1* is a ferroptosis-related gene [14], and its upregulation aggravates acute liver injury through enhancing ferroptosis-mediated lipid peroxides accumulation [15]. However, the role of GAS1 in DR has been poorly researched. Herein, through transcriptome sequencing, GAS1 was discovered to be highly expressed in high glucose (HG)-treated Müller cells, prompting our investigation into the role of GAS1 in DR.

Previous research proved that GAS1 obstructs the transduction of the PI3K/AKT pathway [16,17] which interacts with the Kelch-like ECH-associated protein 1 (Keap1)/nuclear factor erythroid 2-related factor (Nrf2) signaling [18]. Nrf2 is a key regulator of the antioxidant re-

sponse, whose low level is primarily maintained by Keap1-mediated proteasomal degradation under unstressed conditions [19]. Under oxidative stress conditions, Nrf2 protein is stabilized and initiates a multistep pathway of activation that includes nuclear translocation [20]. Nrf2 dissociates from Keap1 and translocates into the nucleus, where it binds to antioxidant response elements, thereby upregulating expressions of downstream antioxidant genes [21]. Moreover, there are evidences that the Keap1/Nrf2 signal prevents the progression of ferroptosis [19,22]. The Keap1/Nrf2 signal activation may protect the retina and alleviate oxidative stress damage during diabetes [23]. Nonetheless, the influence of Keap1/Nrf2 pathway on DR and the participation of GAS1 need further verification.

Accordingly, the current study delved into the effect and potential mechanism based on GAS1-mediated ferroptosis on DR, aiming to provide novel foundations and unravel new biomarkers for DR.

2. Materials and Methods

2.1 Cell Culture and HG Treatment

Rat retinal Müller cells (CP-R117, Procell, Wuhan, China) were cultured in specific DMEM (CM-R117, Procell, Wuhan, China). For high glucose (HG) treatment, the Müller cells were cultured (24 h) in a complete culture medium with 25 mM glucose (G8150, Solarbio, Beijing, China) [24]. After HG/normal glucose (NG) induction, the rat retinal Müller cells were collected and used for transcriptome sequencing. All cell lines were validated by Glutamine Synthetase (GS) immunofluorescence and tested negative for mycoplasma. Cells were all cultured in a humidified incubator (37 °C, 5% CO_2).

2.2 Transcriptome Sequencing

Transcriptome sequencing was performed by the Novogene Company (Novogene, Beijing, China). Sequencing libraries were built using NEBNext® Ultra™ Directional RNA Library Prep Kit (NEB, Ipswich, MA, USA). Briefly, the mRNA was fragmented and purified with poly-T oligo-attached magnetic beads (Beckman Coulter, Brea, CA, USA). Then, first-strand and second-strand cDNAs were synthesized. Polymerase chain reaction (PCR) was performed using universal PCR primers and Index (x) Primer. Finally, the Library preparations were sequenced on an Illumina Hiseq 2000 platform (https://support.illumina.com/sequencing/sequencing_instruments/hiseq_2000/documentation.html). Differential expression analysis, Gene Ontology (GO) enrichment analysis (https://geneontology.org/) and Kyoto Encyclopedia of Genes and Genomes (KEGG) enrichment analysis (https://www.kegg.jp/) were conducted.

2.3 Cell Transfection

Short hairpin RNA (shRNA) for *GAS1* (shGAS1; target sequence: 5′-ACGACTACTACGACGAAGAATAT-3′)/negative control (shNC; target sequence: 5′-AATTCTCCGAACGTGTCACGT-3′), small interference RNA (siRNA) for Nrf2 (siNrf2; si1 target sequence: 5′-CAGCATGATGGACTTGGAATTGC-3′; si2 target sequence: 5′-GGGGTAAGTCGAGAAGTGTTTGA-3′; si3 target sequence: 5′-GGCCTTTTTCGCTCAGTTACAAC-3′), and siNC (target sequence: 5′-TTCTCCGAACGTGTCACGT-3′) were obtained from VectorBuilder (Guangzhou, China). Overexpression plasmids for GAS1 and NC plasmids were synthesized by Sino Biological, Inc. **Supplementary Materia** exhibits coding sequence (CDS) of GAS1. The shRNA, siRNA, or plasmids were transfected (48 h) into Müller cells with 80% density in 6-well plates with transfection reagent (L3000008, Bluefbio, Shanghai, China), followed by cell collection.

2.4 Quantitative Real-time PCR (qRT-PCR) Analysis

Total RNA from Müller cells (a RNA isolation kit; R0017M, Beyotime, Shanghai, China) was detected using the UV spectrophotometer (NanoDrop, Thermo, Waltham, MA, USA) and synthesized into cDNA using First-strand cDNA synthesis kit (D7168M, Beyotime, Shanghai, China), followed by mixing with SYBR green (ALH185, Baiaolaibo, Beijing, China) and primers of a relative gene. The gene expressions were examined by a QuantStudio 6 System (Applied Biosystems, Waltham, MA, USA). Primers' information was as follows: *GAS1* forward (F): 5′-GACCCCGTTTGCCTGTTTTC-3′, reverse (R): 5′-CAGTGCTCCCGATCATCTCC-3′; *Nrf2* F: 5′-TCACACGAGATGAGCTTAGGGCAA-3′, R: 5′-TACAGTTCTGGGCGGCGACTTTAT-3′; *β-actin* F: 5′-CATGTACGTTGCTATCCAGGC-3′, R: 5′-CTCCTTAATGTCACGCACGAT-3′. The relative mRNA expression levels were calculated by $2^{-\Delta\Delta Ct}$ method [25].

2.5 CCK-8 Assay

Transfected/HG-triggered Müller cells (5×10^3) were seeded in 96-well plates (24 h), and then reacted with Cell Counting Kit-8 (CCK-8) reagent (10 µL; 96992, Merk, St. Louis, MO, USA) (2.5 h). Cell viability was gauged through a microplate reader (450 nm; Varioskan LUX, Thermo, Waltham, MA, USA). Cell viability (%) = (optical density $(OD)_{Experimental} - OD_{blank})/(OD_{Control} - OD_{blank}) \times 100$.

2.6 Flow Cytometry

The Annexin V-FITC/propidium iodide (PI) kit (40302ES60, YEASEN, Shanghai, China) was used in this assay. Briefly, transfected/HG-triggered Müller cells were suspended in 100 µL binding buffer, and then incubated with 5 µL Annexin V-FITC and 10 µL PI staining buffer (40302ES60, YEASEN, Shanghai, China) (20 min). Following cell incubation with 400 µL binding buffer, cell apoptosis signal was examined using a flow cytometer (Attune NxT, Thermo, Waltham, MA, USA).

2.7 Detection of Lipid Reactive Oxygen Species (ROS) Level

Post culture of transfected/HG-exposed Müller cells with BODIPY 581/591 C11 (S0043S, Beyotime, Shanghai, China) (20 min, 37 °C) and phosphate buffered saline (PBS) (C0221A, Beyotime, Shanghai, China) washing, lipid ROS levels were assessed using fluorescence microplate reader (GloMax® Discover Microplate Reader, Promega, Madison, WI, USA) (excitation: 581 nm; emission: 591 nm).

2.8 Detection of Glutathione (GSH) and Glutathione Disulfide (GSSG) Levels

GSH and GSSG levels in transfected/HG-exposed Müller cells were evaluated using a total glutathione/oxidized glutathione assay kit (A061-1-2, Nanjing Jiancheng Bioengineering Institute, Nanjing, China). Concretely, the collected Müller cells were ground to pieces, and 10 µL cell samples were mixed with 100 µL reagent 1 and 10 µL reagent 2 (2 min), as well as with 50 µL reagent 3. Then, the OD value was evaluated using a microplate reader (405 nm wavelength) for the calculation of total GSH. Meanwhile, 100 µL cell samples were mixed with 2 µL reagent 5 and 5 µL reagent 6, after which 10 µL mixed solution was further blended with 100 µL reagent 1 and 10 µL reagent 2 (2 min), followed by addition of 50 µL reagent 3. Next, the OD value was evaluated using a microplate reader (405 nm wavelength) for the calculation of GSSG level. Finally, the level of GSH was further calculated as the formula provided by the manufacturer's manual.

2.9 Detection of Malondialdehyde (MDA) Level

MDA levels in transfected/HG-exposed Müller cells were evaluated employing an MDA assay kit (ab118970, Abcam, Cambridge, UK). In brief, the collected Müller cells were mixed with 300 µL MDA lysis buffer and 3 µL BHT stock/BHT, and then underwent centrifugation (13000 $\times g$, 10 min) to obtain the supernatant. Then, 200 µL supernatant and 600 µL developer VII/TBA reagent were cultivated (1 h, 95 °C). Finally, the OD value was detected using a microplate reader (532 nm) for the calculation of the MDA level as the formula provided by manufacturer's instructions.

2.10 Detection of Fe^{2+} Level

Fe^{2+} levels in transfected/HG-exposed Müller cells were evaluated using an Iron assay kit (ab83366, Abcam Cambridge, UK). Briefly, the homogenate of Müller cells (50 µL) experienced incubation with 5 µL iron reducer and 5 µL assay buffer (30 min, 37 °C), followed by culture with 100 µL iron probe (1 h, 37 °C). The OD value was read by a microplate reader (593 nm) for Fe^{2+} level calculation.

2.11 Detection of glutathione S-transferase (GST), Heme Oxygenase-1 (HO-1), and Quinone Oxidoreductase 1 (NQO1) Levels

Quantification of GST, HO-1, and NQO1 in transfected/HG-exposed Müller cells was performed employing GST (ab65326, Abcam, Cambridge, UK), HO-1 (ab279414, Abcam, Cambridge, UK), and NQO1 (ab184867, Abcam, Cambridge, UK) assay kits as per the manual.

2.12 Western Blot

Total protein in transfected/HG-exposed Müller cells was extracted by a RIPA buffer (R0020, Solarbio, Beijing, China) containing a protease inhibitor cocktail (GCPI0015, Vokai Biotechnology, Beijing, China) and PMSF (D16793, Vokai Biotechnology, Beijing, China). The cell nuclear proteins were isolated using a kit (P0027, Beyotime, Shanghai, China) and underwent quantification using a BCA detection kit (KGP903, KeyGEN BioTECH, Nanjing, China). The proteins were incubated with loading buffer (D16796, Vokai Biotechnology, Beijing, China) (5 min, 100 °C), further separated by SDS-PAGE gel (GCPE0017, Vokai Biotechnology, Beijing, China), and transferred to PVDF membrane (YA1701, Solarbio, Beijing, China). The membrane was then incubated with blocking buffer (P0023B, Beyotime, Shanghai, China) overnight, primary antibody overnight (4 °C), and secondary antibody (2 h). By means of ECL luminescent liquid (GCPW0121, Vokai Biotechnology, Beijing, China), the protein bands were detected by a ChemiDoc MP-specific system (Bio-Rad, Hercules, California, USA). The primary and secondary (Beyotime, Shanghai, China) antibodies included Keap1 (60027-1-Ig, 1:4000, Proteintech, Wuhan, China), Nrf2 (20733, 1:1000, CST, Boston, MA, USA), LaminB (66095-1-Ig, 1:20000, Proteintech, Wuhan, China), GAS1 (PA5-101615, 1:1000, Invitrogen, Waltham, MA, USA), β-actin (A2-F6, 1:10000, Huabio, Hangzhou, China), goat anti-rabbit IgG (A0277, 1:3000, Beyotime, Shanghai, China), and goat anti-mouse IgG (A0286, 1:3000, Beyotime, Shanghai, China).

2.13 Statistical Analysis

Data from two groups experienced dissection using independent-sample *t*-test, and those from multiple groups were analyzed using one-way ANOVA by Tukey's post-hoc test using GraphPad 8.0 software (GraphPad Software, San Diego, CA, USA). Measurement data were expressed as mean $\pm$ SD. $p < 0.05$ meant statistical significance.

3. Results

3.1 HG Treatment Decreased the Viability, and Increased Apoptosis, Lipid Peroxidation and Fe^{2+} Levels in Müller Cells

HG treatment resulted in decreased viability of Müller cells ($p < 0.01$, Fig. 1A) and increased apoptosis ($p < 0.001$, Fig. 1B,C). Subsequently, the lipid peroxidation in

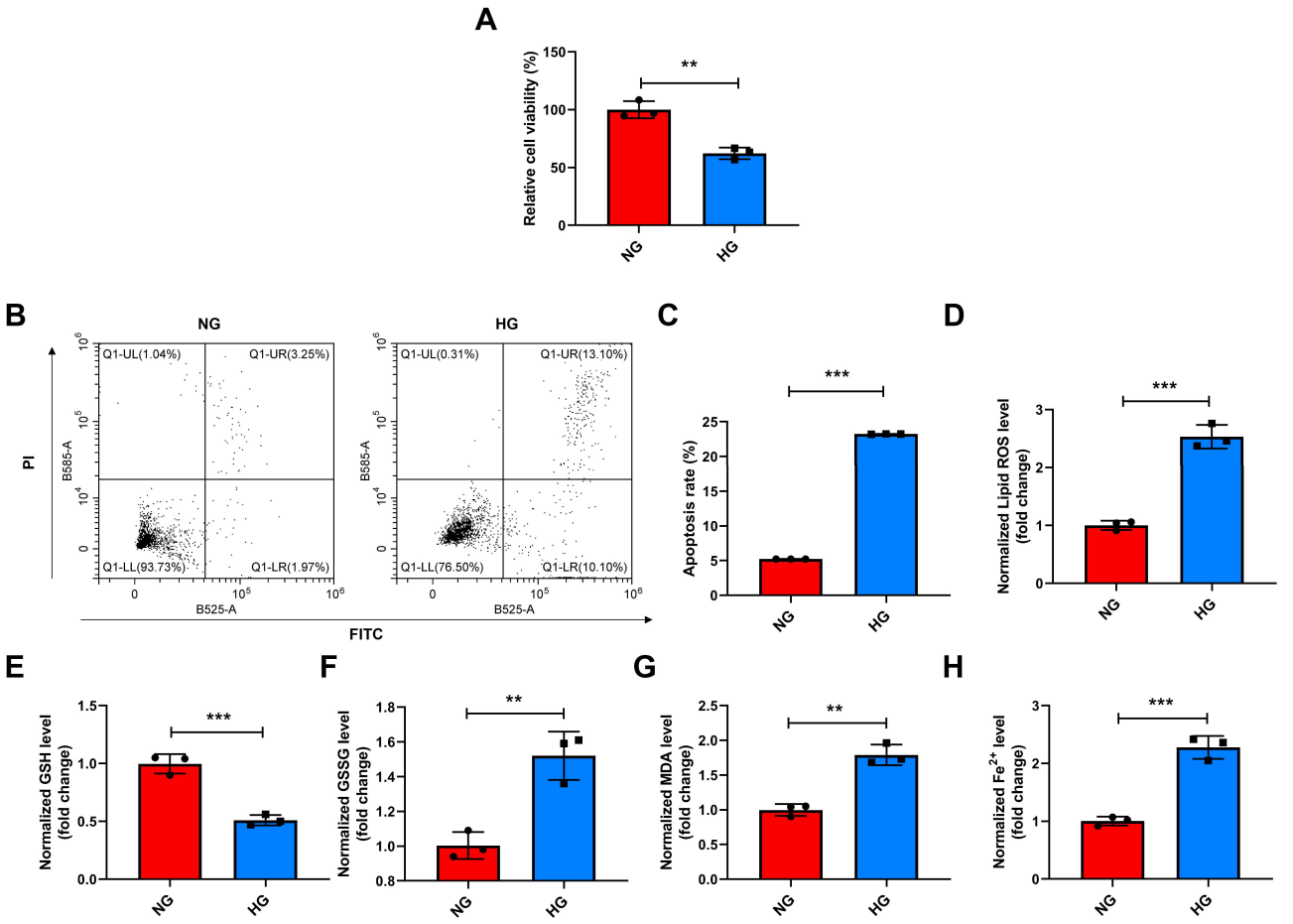

Fig. 1. HG treatment decreased the viability and increased apoptosis, lipid peroxidation, and Fe^{2+} levels in Müller cells. (A–H) The viability (CCK-8) assay (A), the apoptosis (flow cytometry) (B,C), and the levels of lipid ROS, GSH, GSSG, MDA, and Fe^{2+} (commercial reagent kit) (D–H) in HG-exposed (24 h) Müller cells. $^{**}p < 0.01$, $^{***}p < 0.001$ vs. NG. CCK-8, Cell Counting Kit-8; NG, normal glucose; HG, high glucose; ROS, reactive oxygen species; GSH, glutathione; GSSG, glutathione disulfide; MDA, malondialdehyde. n = 3 in each group.

Müller cells was evaluated. As shown in Fig. 1D–G, the lipid ROS, GSSG, and MDA in HG-treated Müller cells were elevated ($p < 0.01$), and the GSH was reduced ($p < 0.001$). Furthermore, the Fe^{2+} level in Müller cells was raised by HG treatment ($p < 0.001$, Fig. 1H). These results revealed that HG treatment decreased the viability and increased apoptosis, lipid peroxidation, and Fe^{2+} level in Müller cells.

3.2 GAS1 was Differentially Expressed in HG-treated Müller Cells

In HG-exposed Müller cells, transcriptome sequencing data unveiled many differentially expressed genes (DEGs) (Fig. 2A,B), with 34 downregulated genes and 339 upregulated genes in line with the volcano plot. GAS1 level was lower in NG-treated Müller cells than HG-treated Müller cells (Fig. 2B). GO analysis provided insights into the biological process (BP), molecular function (MF), and cell component (CC) of DEG's enrichment (Fig. 3A). Meanwhile, KEGG's enrichment results show that Glycosphingolipid Biosynthesis-globo and isoglobo Series, Motor proteins and selenocompound metabolism is the top three metabolic channels of the enrichment (Fig. 3B). Furthermore, *GAS1* expression in HG-treated Müller cells was discovered to be upregulated ($p < 0.001$, Fig. 3C).

3.3 GAS1 Downregulation Promoted the Viability and Inhibited the Apoptosis and Oxidative Stress of HG-treated Müller Cells

To evaluate how GAS1 impacted HG-treated Müller cells, shGAS1 was transfected into Müller cells. Fig. 4A–C revealed increased GAS1 expression by HG treatment ($p < 0.001$), while shGAS1 reversed the role of HG ($p < 0.001$). Through CCK-8 and flow cytometry assays, it was discovered that HG treatment attenuated viability ($p < 0.001$, Fig. 4D) and enhanced apoptosis ($p < 0.001$, Fig. 4E,F) of Müller cells, but shGAS1 offset these effects of HG ($p < 0.001$). Besides, detection of oxidative stress (Fig. 4G–I)

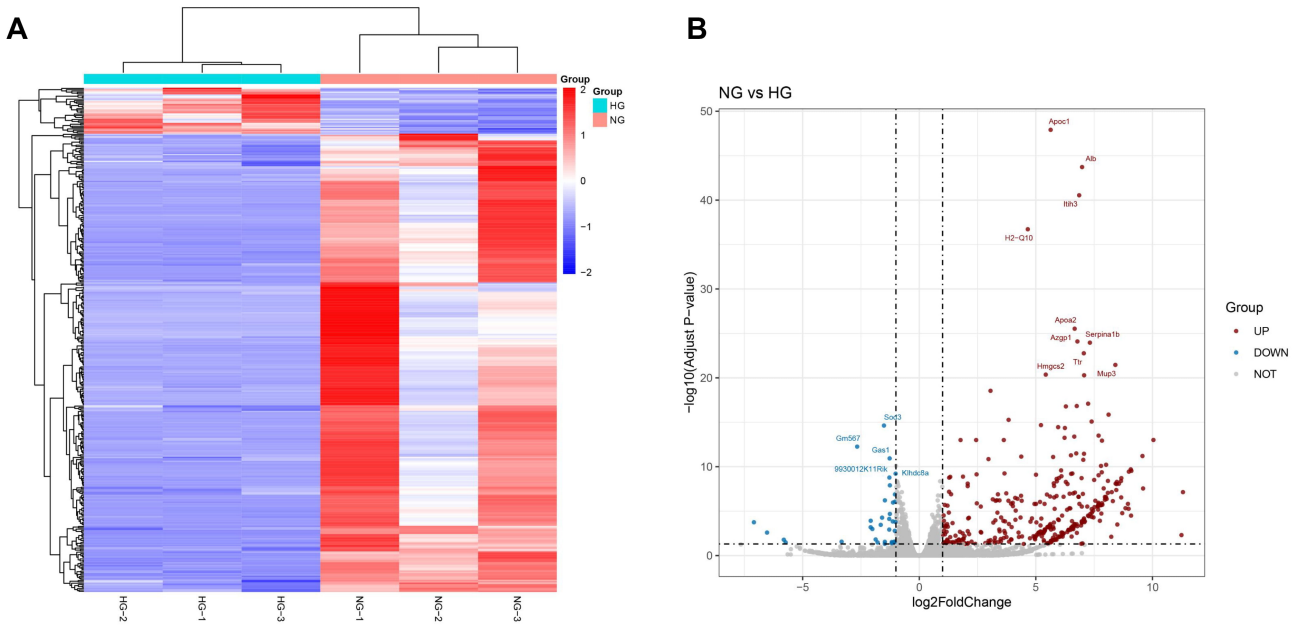

Fig. 2. GAS1 was differentially expressed in HG-treated Müller cells. (A,B) Heat map (A) and volcano map (B) of NG/HG-treated (24 h) DEGs in Müller cells (transcriptome sequencing), showing decreased GAS1 expression in the NG group relative to HG group. NG, normal glucose; HG, high glucose; GAS1, growth arrest-specific 1; DEGs, differentially expressed genes.

proved HG induction augmented concentrations of GST, HO-1 and NQO1 in Müller cells ($p < 0.001$), while GAS1 downregulation reduced GST, HO-1 and NQO1 levels following HG treatment ($p < 0.001$). The above discovers revealed that GAS1 downregulation promoted the viability and inhibited the apoptosis and oxidative stress of HG-treated Müller cells.

3.4 GAS1 Downregulation Reduced the Lipid Peroxidation and Fe^{2+} Levels of HG-treated Müller Cells

Then, examination of lipid peroxidation (Fig. 5A–D) indicated the relative levels of lipid ROS, GSSG, and MDA were increased ($p < 0.01$), while the GSH level was reduced ($p < 0.001$) in Müller cells due to HG treatment; however, the role of HG was offset by shGAS1 ($p < 0.001$). Meanwhile, the Fe^{2+} level in HG-treated Müller cells was increased ($p < 0.001$, Fig. 5E), which was counteracted by shGAS1 ($p < 0.001$, Fig. 5E).

3.5 GAS1 Downregulation Promoted the Keap1/Nrf2 Signal in HG-treated Müller Cells

Mechanistically, Keap1/Nrf2 signaling transduction was evaluated (Fig. 6A–D), revealing upregulated Keap1 and total Nrf2 as well as downregulated nuclear Nrf2 in HG-treated Müller cells ($p < 0.001$), which however were all reversed after shGAS1 transfection ($p < 0.001$). These findings suggested that GAS1 downregulation promoted Keap1/Nrf2 signal in HG-treated Müller cells.

3.6 Nrf2 Deficiency Reversed the Role of GAS1 in the Viability, Apoptosis, and Oxidative Stress of HG-treated Müller Cells

To confirm that GAS1 impacted HG-treated Müller cells through regulating the Keap1/Nrf2 signal, Nrf2 was silenced in Müller cells ($p < 0.05$, Fig. 7A–C). Due to the highest transfection efficiency, si2 was chosen for later use. Meanwhile, GAS1 was also overexpressed in Müller cells ($p < 0.001$, Fig. 7D–F). In HG-treated Müller cells, GAS1 overexpression weakened viability ($p < 0.001$, Fig. 7G) and induced apoptosis ($p < 0.001$, Fig. 7H,I), which were reversed by Nrf2 silencing ($p < 0.01$, Fig. 7G–I). Moreover, detection of oxidative stress revealed that GAS1 overexpression raised the concentrations of GST, HO-1, and NQO1 in HG-treated Müller cells ($p < 0.05$, Fig. 7J–L), which were further offset by Nrf2 silencing ($p < 0.05$, Fig. 7J–L). Accordingly, it was conjectured that GAS1 may mediate Keap1/Nrf2 signal to impact viability, apoptosis, and oxidative stress of HG-treated Müller cells.

3.7 Nrf2 Deficiency Reversed the Role of GAS1 in the Lipid Peroxidation and Fe^{2+} Levels of HG-treated Müller Cells

Changes in lipid peroxidation and Fe^{2+} levels in HG-treated Müller cells were examined (Fig. 8A–D). GAS1 overexpression increased lipid ROS production, GSSG level and MDA level ($p < 0.01$), and reduced GSH level in HG-treated Müller cells ($p < 0.01$); however, Nrf2 silencing counteracted these impacts of GAS1 ($p < 0.01$). Meanwhile, the Fe^{2+} level of HG-treated Müller cells was upregulated by GAS1 overexpression ($p < 0.001$, Fig. 8E), which was then offset by Nrf2 downregulation ($p < 0.001$,

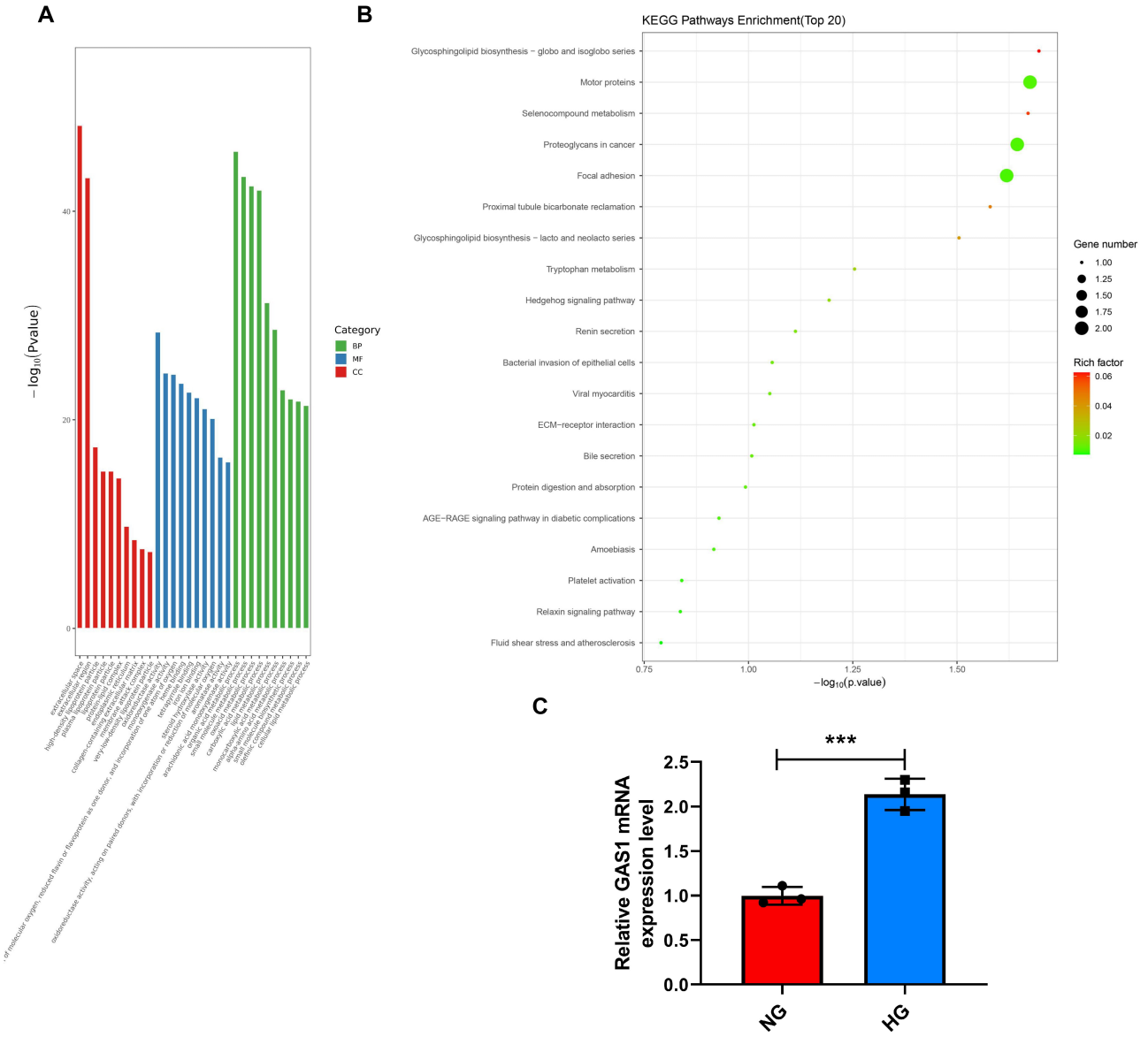

Fig. 3. GAS1 was upregulated in HG-treated Müller cells. (A,B) BP, MF, and CC of enrichment between GO and KEGG of DEGs (A) and the pathways enrichment between GO and KEGG of DEGs (B) (GO and KEGG analysis). (C) *GAS1* expression in HG-exposed (24 h) Müller cells (quantitative real-time PCR). ***$p < 0.001$ vs. NG. NG, normal glucose; HG, high glucose; GAS1, growth arrest-specific 1; BP, biological process; MF, molecular function; CC, cellular componenta. n = 3 in each group.

Fig. 8E). We thus inferred that GAS1 impacted lipid peroxidation and Fe^{2+} levels of HG-treated Müller cells by regulating Keap1/Nrf2 signal.

3.8 Nrf2 Deficiency Reversed the Role of GAS1 in Keap1/Nrf2 Signaling Transduction in HG-treated Müller Cells

Finally, Keap1/Nrf2 signaling transduction was evaluated (Fig. 9A–D). The expressions of Keap1 and total Nrf2 were upregulated while nuclear Nrf2 expression was downregulation in HG-treated Müller cells after GAS1 overexpression ($p < 0.001$); however, the effects of GAS1 overexpression were all neutralized by Nrf2 deficiency ($p < 0.001$). These outcomes further confirmed that GAS1 can repress Keap1/Nrf2 signaling transduction.

4. Discussion

This research uncovered that GAS1 expression, lipid ROS, GSSG, MDA, oxidative stress, and ferroptosis were boosted, and the Keap1/Nrf2 signal was inhibited in HG-exposed Müller cells. GAS1 downregulation increased the viability and GSH level, reduced the lipid ROS, GSSG, MDA, oxidative stress and ferroptosis, and promoted Keap1/Nrf2 signal in HG-treated Müller cells, while GAS1 overexpression did oppositely. Nrf2 silencing reversed the role of GAS1 overexpression in HG-treated Müller cells.

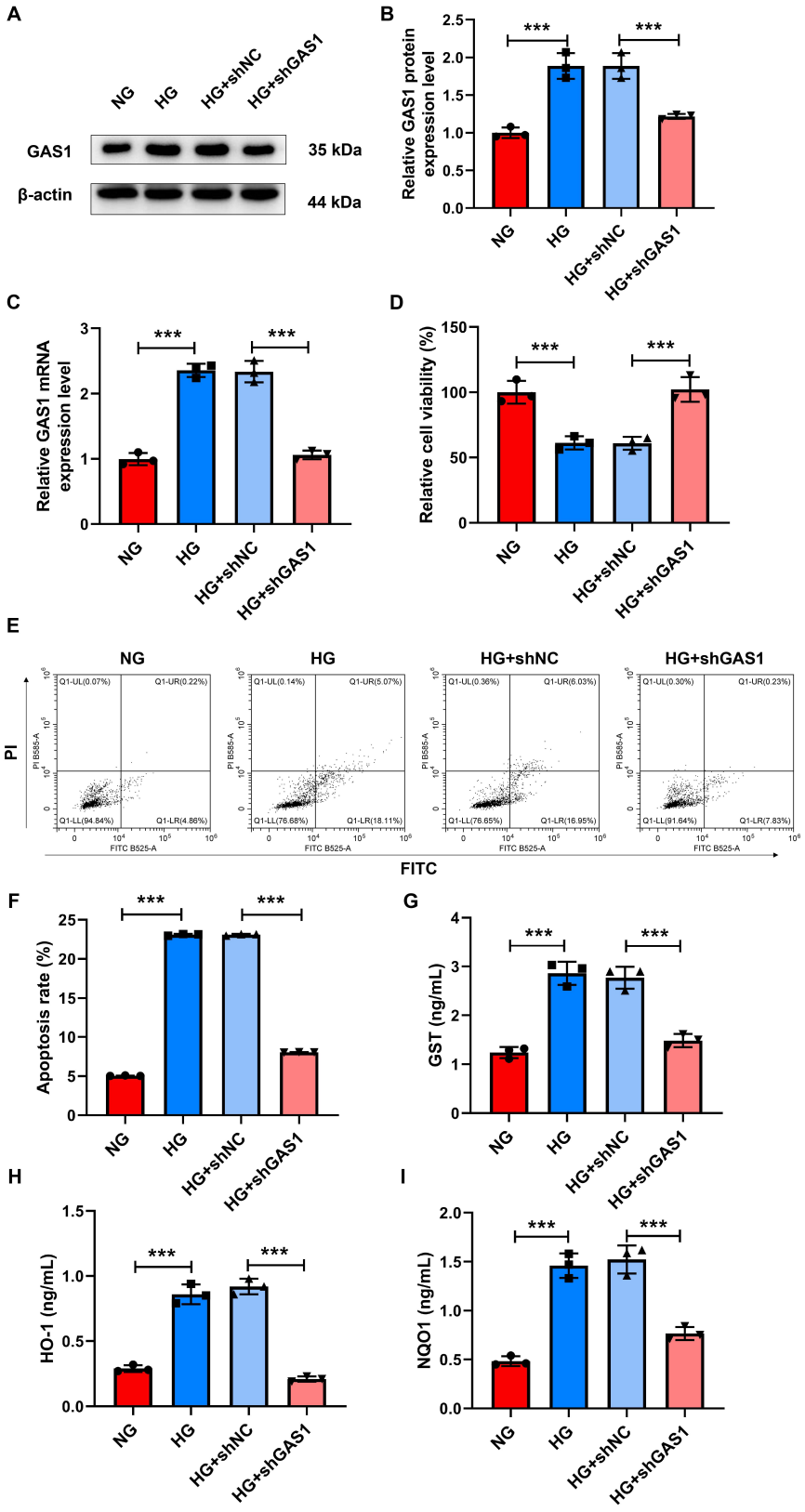

Fig. 4. GAS1 downregulation promoted the viability and inhibited the apoptosis and oxidative stress of HG-treated Müller cells. (A–I) GAS1 expression (western blotting and quantitative real-time PCR) (A–C), viability (CCK-8 assay) (D), apoptosis (flow cytometry) (E,F), and the concentrations of GST, HO-1, and NQO1 (commercial reagent kit) (G–I) in shGAS1-transfected and HG-treated Müller cells. ***$p < 0.001$. NG, normal glucose; HG, high glucose; GAS1, growth arrest-specific 1; GST, glutathione-s-transferase; HO-1, heme oxygenase-1; NQO1, quinone oxidoreductase 1; shNC; negative control for shGAS1. n = 3 in each group.

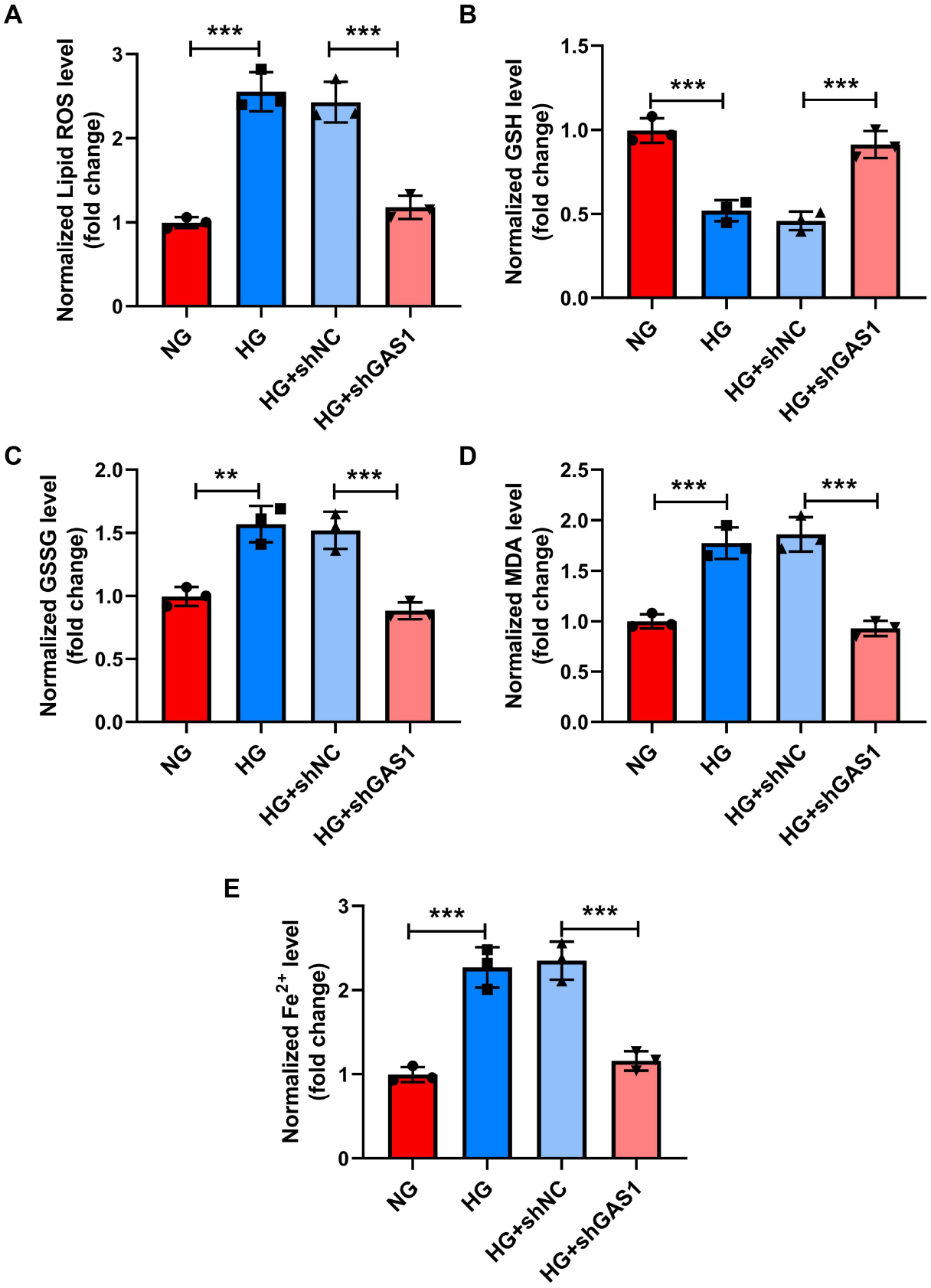

Fig. 5. GAS1 downregulation reduced the lipid peroxidation and Fe^{2+} levels of HG-treated Müller cells. (A–E) Levels of lipid ROS, GSH, GSSG, MDA, and Fe^{2+} in shGAS1-transfected and HG-treated Müller cells (commercial reagent kit). $^{**}p < 0.01$, $^{***}p < 0.001$. NG, normal glucose; HG, high glucose; GAS1, growth arrest-specific 1; ROS, reactive oxygen species; GSH, glutathione; GSSG, glutathione disulfide; MDA, malondialdehyde; shNC; negative control for shGAS1. n = 3 in each group.

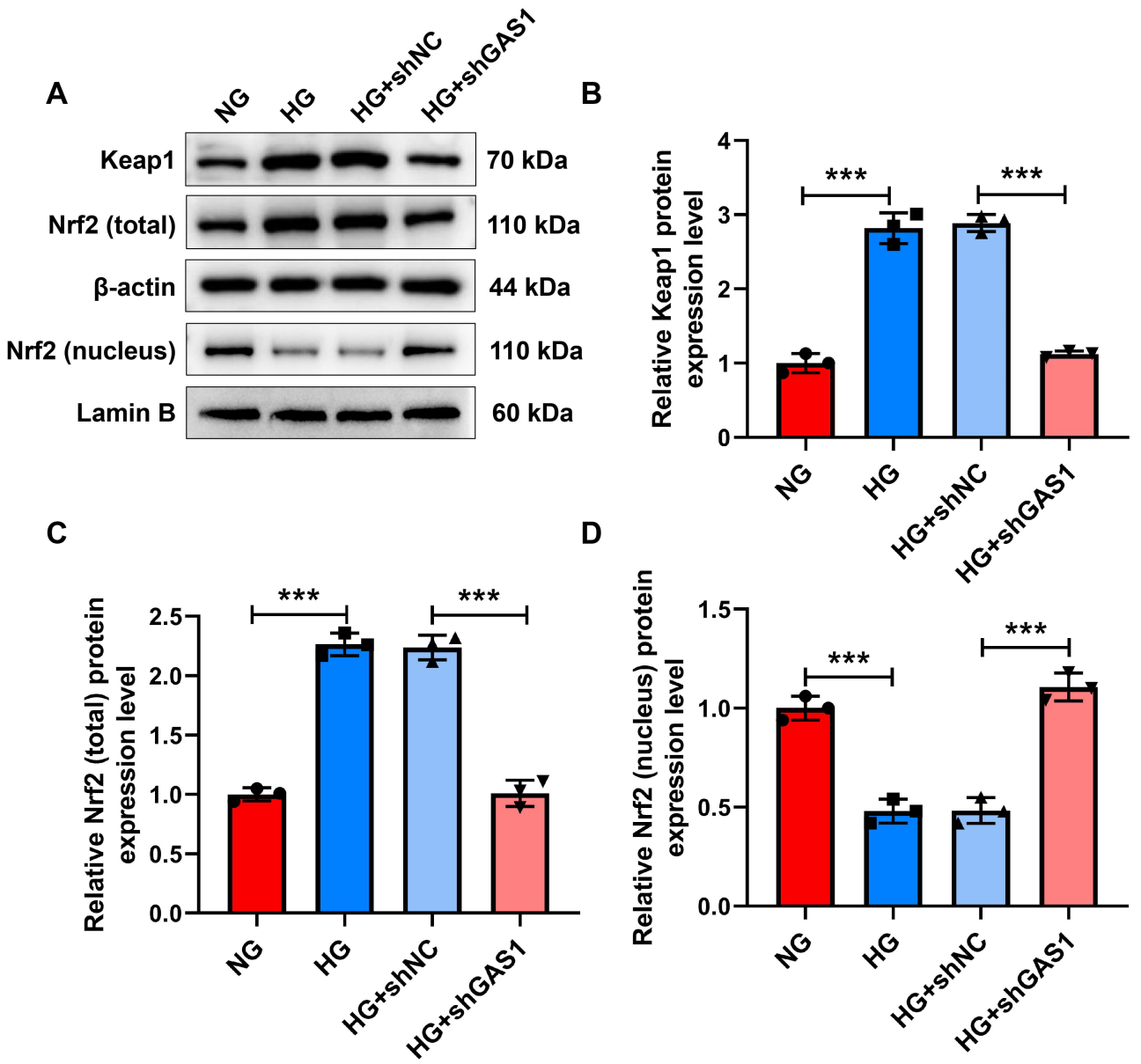

Fig. 6. GAS1 downregulation promoted the Keap1/Nrf2 signal in HG-treated Müller cells. (A–D) Expressions of Keap1, total Nrf2, and nuclear Nrf2 in shGAS1-transfected and HG-treated Müller cells (Western blot). ***$p < 0.001$. NG, normal glucose; HG, high glucose; GAS1, growth arrest-specific 1; Keap1, Kelch-like ECH-associated protein 1; Nrf2, nuclear factor erythroid 2-related factor; shNC, negative control for shGAS1. n = 3 in each group.

This work proved that GAS1 impeded Keap1/Nrf2 signaling transduction to activate ferroptosis in retinal Müller cells.

Ferroptosis, a newly discovered cell death reliant on iron regulation [26,27], has the main feature of excess iron deposition that elevates ROS and oxidative stress, further promoting lipid peroxidation [28,29]. Abundant evidence identified diabetes is intimately pertinent to ferroptosis [9,30–32]. Hyperglycemia contributes to excessive production of ROS, further causing oxidative stress in various organs of diabetes patients [33]. HG results in iron overload and dysregulation, and then induces oxidative stress and lipid peroxidation containing ROS production, GSSG and MDA accumulation, and GSH reduction, ultimately initiating ferroptosis [34–36]. Herein, after HG treatment, the viability and GSH were decreased while the apoptosis, ROS, GSSG, MDA, Fe^{2+}, GST, HO-1, and NQO1 were increased in rat Müller cells, suggesting that HG induced ferroptosis in rat Müller cells.

As a multifunctional protein, GAS1 possesses regulatory effects on various diseases, and its activation in human brain tumor-initiating cells can reduce the tumorigenecity [37], while its loss enhances the degeneration of nucleus pulposus tissues [38]. Besides, GAS1 is discovered to be

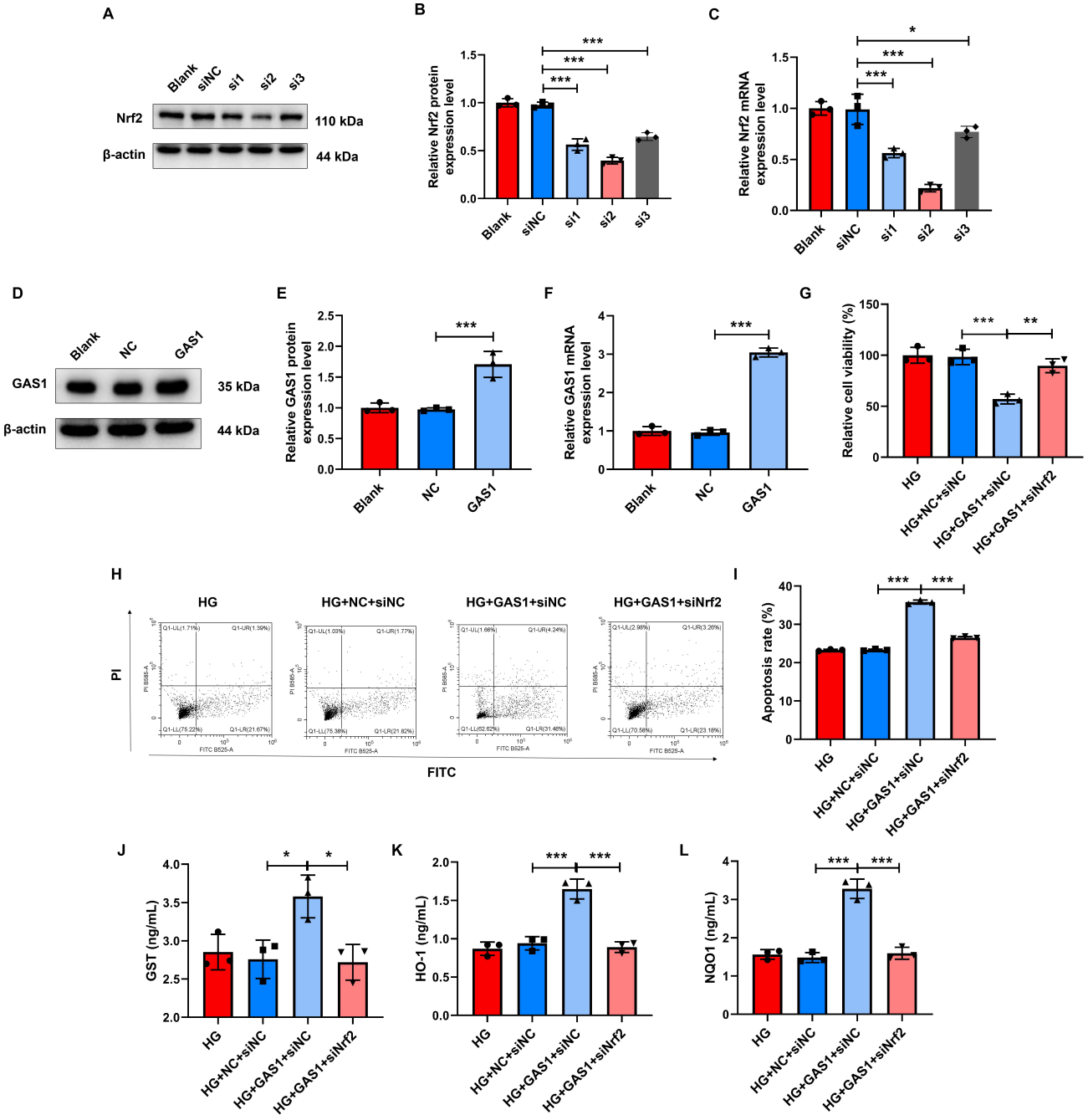

Fig. 7. Nrf2 downregulation reversed the role of GAS1 in the viability, apoptosis, and oxidative stress of HG-treated Müller cells. (A–C) The transfection efficiency of siRNA for Nrf2 and (D–F) GAS1 overexpression plasmids (western blotting and quantitative real-time PCR). (G–L) Viability (CCK-8 assay) (G), apoptosis (flow cytometry) (H–I), and the concentrations of GST, HO-1, and NQO1 (commercial reagent kit) (J–L) in transfected and HG-exposed Müller cells. *$p < 0.05$, **$p < 0.01$, ***$p < 0.001$. HG, high glucose; GAS1, growth arrest-specific 1; HO-1, heme oxygenase-1; NQO1, quinone oxidoreductase 1; Nrf2, nuclear factor erythroid 2-related factor; NC, negative control for GAS1 overexpression plasmid; siNC, negative control for siNrf2. n = 3 in each group.

a specific marker in diabetic rats and is highly expressed in diabetes, which has a crucial effect on the maintenance and differentiation of principal cells in diabetic nephropathy [39]. Herein, we provided new discovery that GAS1 was highly expressed in HG-exposed rat Müller cells. Furthermore, GAS1 can trigger cell death by an intrinsic apoptotic pathway [13]. GAS1 is a ferroptosis-related gene in high-grade serous ovarian cancer [14], and GAS1 upregulation aggravates acute liver injury through enhancing ferroptosis-mediated lipid peroxides accumulation [15]. Herein, we verified deficient GAS1 increased the viability and GSH while reducing the apoptosis, ROS, GSSG, MDA, Fe^{2+},

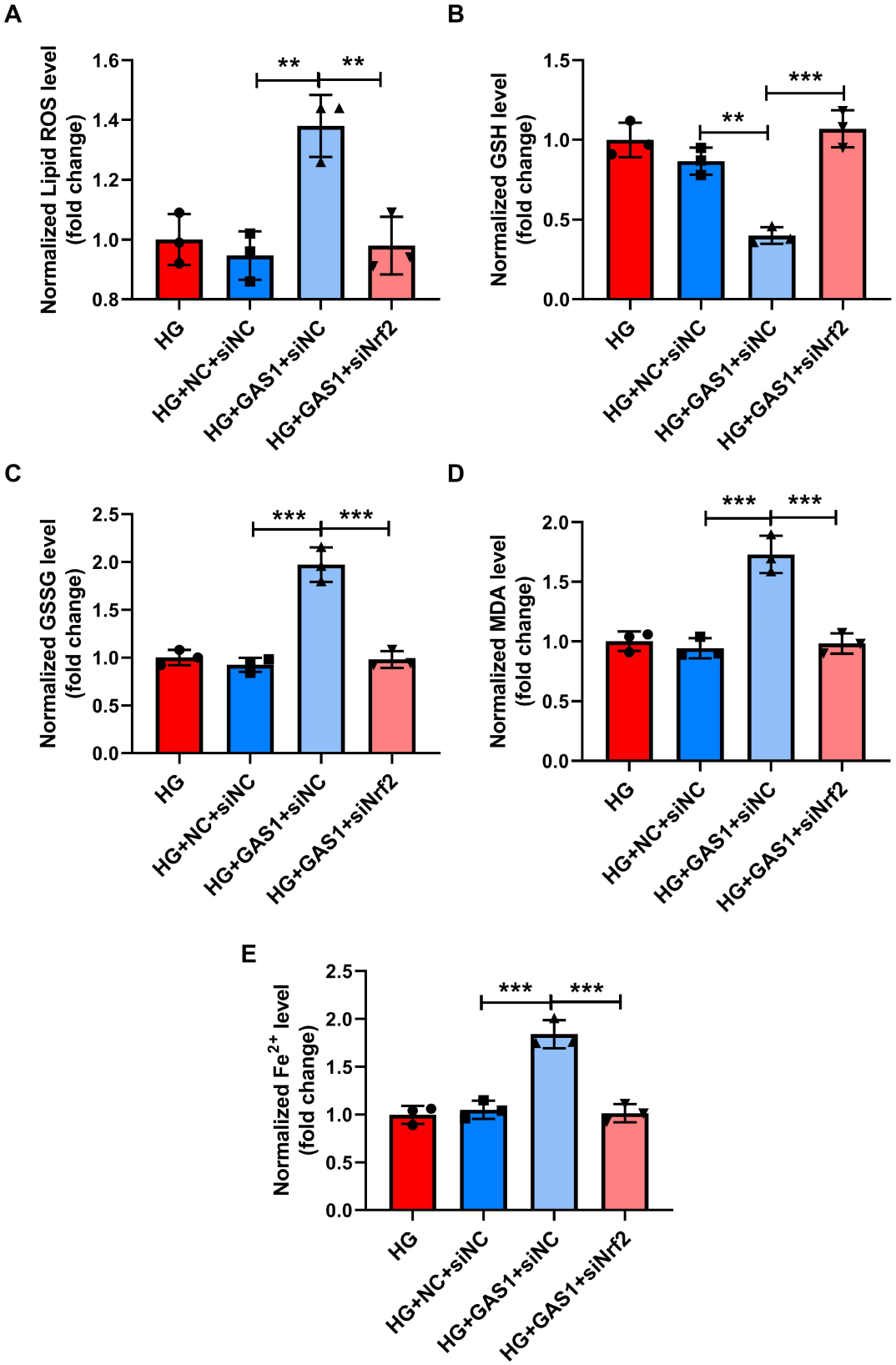

Fig. 8. Nrf2 downregulation reversed the role of GAS1 in the lipid peroxidation and Fe^{2+} levels of HG-treated Müller cells. (A–E) Levels of lipid ROS, GSH, GSSG, MDA, and Fe^{2+} in transfected and HG-exposed Müller cells (commercial reagent kit). $^{**}p < 0.01$, $^{***}p < 0.001$. HG, high glucose; GAS1, growth arrest-specific 1; ROS, reactive oxygen species; GSH, glutathione; GSSG, glutathione disulfide; MDA, malondialdehyde; Nrf2, nuclear factor erythroid 2-related factor; NC, negative control for GAS1 overexpression plasmid; siNC, negative control for siNrf2. n = 3 in each group.

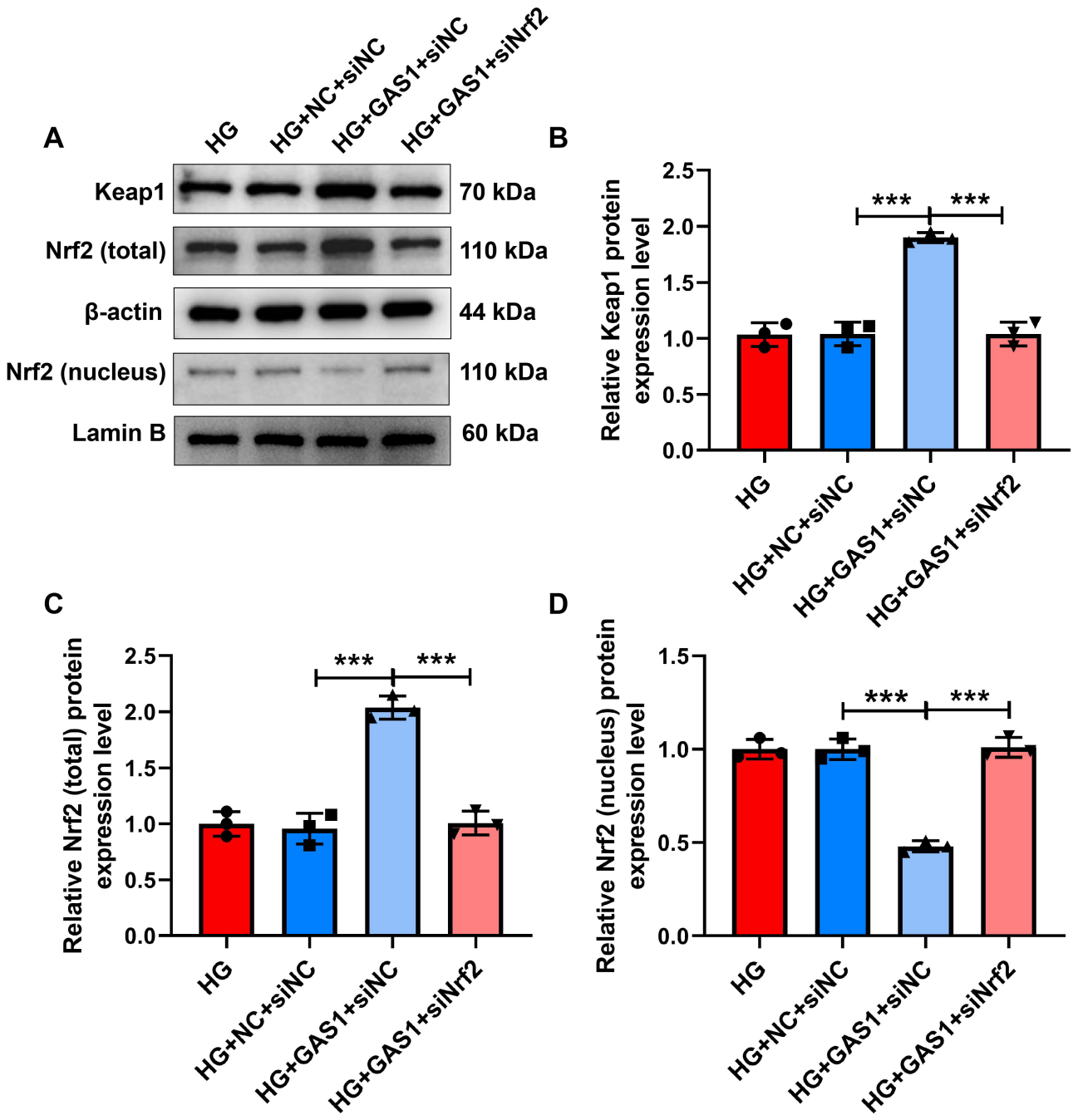

Fig. 9. Nrf2 downregulation reversed the role of GAS1 in Keap1/Nrf2 signaling transduction in HG-treated Müller cells. (A–D) Expressions of Keap1, total Nrf2, and nuclear Nrf2 in transfected and HG-exposed Müller cells (Western blot). ***$p < 0.001$. HG, high glucose; GAS1, growth arrest-specific 1; Keap1, Kelch-like ECH-associated protein 1; Nrf2, nuclear factor erythroid 2-related factor; NC, negative control for GAS1 overexpression plasmid; siNC, negative control for siNrf2. n = 3 in each group.

GST, HO-1, and NQO1 in rat Müller cells, but GAS1 overexpression did the opposite, revealing that GAS1 upregulation promoted while GAS1 downregulation inhibited the ferroptosis in HG-treated rat Müller cells.

Reportedly, GAS1 obstructs PI3K/AKT pathway transduction [16,17] which interacts with the Keap1/Nrf2 signaling [18]. Moreover, the Keap1/Nrf2 signal prevents the progression of ferroptosis [19,22]. The Keap1/Nrf2 pathway is the main protective response to oxidant and electrophilic stress. Under homeostatic conditions, Keap1 targets Nrf2 for ubiquitination and proteasome dependent degradation, strictly regulating the activity of Nrf2; in stress response, the complex molecular mechanism promoted by the cysteine sensor in Keap1 allows Nrf2 to evade ubiquitination, accumulate in cells, and transport to the nucleus, where it can promote its antioxidant transcription program

[40]. In DR model cells, the nuclear translocation and expression of Nrf2 is the activation of the Keap1/Nrf2 pathway induced by Acteoside, contributing to inhibition of the HG-induced oxidative stress injury [41]. In this work, the expressions of Keap1 and total Nrf2 were decreased, while nuclear Nrf2 expression was increased by GAS1 knockdown in HG-treated Müller cells, but GAS1 overexpression generated opposite effects, revealing that GAS1 overexpression inhibited while GAS1 downregulation promoted the transduction of the Keap1/Nrf2 signaling. Additionally, Nrf2 silencing abrogated GAS1 overexpression-induced ferroptosis in HG-treated rat Müller cells, further proving that the role of GAS1 in ferroptosis in DR was realized by regulating Keap1/Nrf2 signaling. Of note, some limitations exist and require resolution. Firstly, the effect of GAS1 on HG-treated Müller cells was only verified at the cellular level, necessitating animal experiments and clinical experiments. Secondly, we only analyzed the effect of GAS1 on HG-exposed Müller cells, and its effect on other biological behaviors of Müller cells remains obscure. Hence, we will explore the role of GAS1 in other cells and the effect of GAS1 on other biological functions in our future work.

5. Conclusion

Collectively, this work finds that GAS1 is upregulated in HG-exposed Müller cells, which can inhibit Keap1/Nrf2 signaling transduction to activate ferroptosis in retinal Müller cells. Our findings provide important clues for new drug development, optimize existing treatments, and offer novel foundation and biomarkers for DR treatment to improve therapeutic efficacy. Nevertheless, additional evidence and further experiments are necessary to substantiate our findings.

Availability of Data and Materials

The analyzed data sets generated during the study are available from the corresponding author on reasonable request.

Author Contributions

Substantial contributions to conception and design: RFD. Data acquisition, data analysis and interpretation: YQ, SQL, XZ, SSS, ZS. Drafting the article or critically revising it for important intellectual content: All authors. Final approval of the version to be published: All authors. Agreement to be accountable for all aspects of the work in ensuring that questions related to the accuracy or integrity of the work are appropriately investigated and resolved: All authors.

Ethics Approval and Consent to Participate

Not applicable.

Acknowledgment

Not applicable.

Funding

This research received no external funding.

Conflict of Interest

The authors declare no conflict of interest.

Supplementary Material

Supplementary material associated with this article can be found, in the online version, at https://doi.org/10.31083/FBL27954.

References

[1] Huang X, Wang H, She C, Feng J, Liu X, Hu X, *et al*. Artificial intelligence promotes the diagnosis and screening of diabetic retinopathy. Frontiers in Endocrinology. 2022; 13: 946915. https://doi.org/10.3389/fendo.2022.946915.

[2] GBD 2019 Blindness and Vision Impairment Collaborators, Vision Loss Expert Group of the Global Burden of Disease Study. Causes of blindness and vision impairment in 2020 and trends over 30 years, and prevalence of avoidable blindness in relation to VISION 2020: the Right to Sight: an analysis for the Global Burden of Disease Study. The Lancet. Global Health. 2021; 9: e144–e160. https://doi.org/10.1016/S2214-109X(20)30489-7.

[3] Oh K, Kang HM, Leem D, Lee H, Seo KY, Yoon S. Early detection of diabetic retinopathy based on deep learning and ultra-wide-field fundus images. Scientific Reports. 2021; 11: 1897. https://doi.org/10.1038/s41598-021-81539-3.

[4] Yang J, Liu Z. Mechanistic Pathogenesis of Endothelial Dysfunction in Diabetic Nephropathy and Retinopathy. Frontiers in Endocrinology. 2022; 13: 816400. https://doi.org/10.3389/fendo.2022.816400.

[5] Porta M, Striglia E. Intravitreal anti-VEGF agents and cardiovascular risk. Internal and Emergency Medicine. 2020; 15: 199–210. https://doi.org/10.1007/s11739-019-02253-7.

[6] Kataoka SY, Lois N, Kawano S, Kataoka Y, Inoue K, Watanabe N. Fenofibrate for diabetic retinopathy. The Cochrane Database of Systematic Reviews. 2023; 6: CD013318. https://doi.org/10.1002/14651858.CD013318.pub2.

[7] Jiang X, Stockwell BR, Conrad M. Ferroptosis: mechanisms, biology and role in disease. Nature Reviews. Molecular Cell Biology. 2021; 22: 266–282. https://doi.org/10.1038/s41580-020-00324-8.

[8] Zeng F, Nijiati S, Tang L, Ye J, Zhou Z, Chen X. Ferroptosis Detection: From Approaches to Applications. Angewandte Chemie (International Ed. in English). 2023; 62: e202300379. https://doi.org/10.1002/anie.202300379.

[9] Liu P, Zhang Z, Cai Y, Li Z, Zhou Q, Chen Q. Ferroptosis: Mechanisms and role in diabetes mellitus and its complications. Ageing Research Reviews. 2024; 94: 102201. https://doi.org/10.1016/j.arr.2024.102201.

[10] Liu C, Sun W, Zhu T, Shi S, Zhang J, Wang J, *et al*. Glia maturation factor-β induces ferroptosis by impairing chaperone-mediated autophagic degradation of ACSL4 in early diabetic retinopathy. Redox Biology. 2022; 52: 102292. https://doi.org/10.1016/j.redox.2022.102292.

[11] Fan X, Xu M, Ren Q, Fan Y, Liu B, Chen J, *et al*. Downregulation of fatty acid binding protein 4 alleviates lipid peroxidation and oxidative stress in diabetic retinopathy by regulating peroxisome proliferator-activated receptor γ-mediated ferropto-

sis. Bioengineered. 2022; 13: 10540–10551. https://doi.org/10.1080/21655979.2022.2062533.
[12] Ayala-Sarmiento AE, Estudillo E, Pérez-Sánchez G, Sierra-Sánchez A, González-Mariscal L, Martínez-Fong D, *et al*. GAS1 is present in the cerebrospinal fluid and is expressed in the choroid plexus of the adult rat. Histochemistry and Cell Biology. 2016; 146: 325–336. https://doi.org/10.1007/s00418-016-1449-0.
[13] Zarco N, González-Ramírez R, González RO, Segovia J. GAS1 induces cell death through an intrinsic apoptotic pathway. Apoptosis: an International Journal on Programmed Cell Death. 2012; 17: 627–635. https://doi.org/10.1007/s10495-011-0696-8.
[14] Sun X, He W, Lin B, Huang W, Ye D. Defining three ferroptosis-based molecular subtypes and developing a prognostic risk model for high-grade serous ovarian cancer. Aging. 2024; 16: 9106–9126. https://doi.org/10.18632/aging.205857.
[15] Tao J, Xue C, Wang X, Chen H, Liu Q, Jiang C, *et al*. GAS1 Promotes Ferroptosis of Liver Cells in Acetaminophen-Induced Acute Liver Failure. International Journal of Medical Sciences. 2023; 20: 1616–1630. https://doi.org/10.7150/ijms.85114.
[16] Dong C, Wang X, Li N, Zhang K, Wang X, Zhang H, *et al*. microRNA-mediated *GAS1* downregulation promotes the proliferation of synovial fibroblasts by PI3K-Akt signaling in osteoarthritis. Experimental and Therapeutic Medicine. 2019; 18: 4273–4286. https://doi.org/10.3892/etm.2019.8101.
[17] Ma Y, Qin H, Cui Y. MiR-34a targets GAS1 to promote cell proliferation and inhibit apoptosis in papillary thyroid carcinoma via PI3K/Akt/Bad pathway. Biochemical and Biophysical Research Communications. 2013; 441: 958–963. https://doi.org/10.1016/j.bbrc.2013.11.010.
[18] Zhang Q, Yao M, Qi J, Song R, Wang L, Li J, *et al*. Puerarin inhibited oxidative stress and alleviated cerebral ischemia-reperfusion injury through PI3K/Akt/Nrf2 signaling pathway. Frontiers in Pharmacology. 2023; 14: 1134380. https://doi.org/10.3389/fphar.2023.1134380.
[19] Sun X, Ou Z, Chen R, Niu X, Chen D, Kang R, *et al*. Activation of the p62-Keap1-NRF2 pathway protects against ferroptosis in hepatocellular carcinoma cells. Hepatology (Baltimore, Md.). 2016; 63: 173–184. https://doi.org/10.1002/hep.28251.
[20] Suzuki T, Motohashi H, Yamamoto M. Toward clinical application of the Keap1-Nrf2 pathway. Trends in Pharmacological Sciences. 2013; 34: 340–346. https://doi.org/10.1016/j.tips.2013.04.005.
[21] Mirzaei S, Zarrabi A, Hashemi F, Zabolian A, Saleki H, Azami N, *et al*. Nrf2 Signaling Pathway in Chemoprotection and Doxorubicin Resistance: Potential Application in Drug Discovery. Antioxidants (Basel, Switzerland). 2021; 10: 349. https://doi.org/10.3390/antiox10030349.
[22] Luo X, Wang Y, Zhu X, Chen Y, Xu B, Bai X, *et al*. MCL attenuates atherosclerosis by suppressing macrophage ferroptosis via targeting KEAP1/NRF2 interaction. Redox Biology. 2024; 69: 102987. https://doi.org/10.1016/j.redox.2023.102987.
[23] Li X, Deng A, Liu J, Hou W. The role of Keap1-Nrf2-ARE signal pathway in diabetic retinopathy oxidative stress and related mechanisms. International Journal of Clinical and Experimental Pathology. 2018; 11: 3084–3090.
[24] Vellanki S, Ferrigno A, Alanis Y, Betts-Obregon BS, Tsin AT. High Glucose and Glucose Deprivation Modulate Müller Cell Viability and VEGF Secretion. International Journal of Ophthalmology & Eye Science. 2016; 4: 178–183.
[25] Livak KJ, Schmittgen TD. Analysis of relative gene expression data using real-time quantitative PCR and the 2(-Delta Delta C(T)) Method. Methods (San Diego, Calif.). 2001; 25: 402–408. https://doi.org/10.1006/meth.2001.1262.
[26] Li J, Cao F, Yin HL, Huang ZJ, Lin ZT, Mao N, *et al*. Ferroptosis: past, present and future. Cell Death & Disease. 2020; 11: 88. https://doi.org/10.1038/s41419-020-2298-2.
[27] Liang D, Minikes AM, Jiang X. Ferroptosis at the intersection of lipid metabolism and cellular signaling. Molecular Cell. 2022; 82: 2215–2227. https://doi.org/10.1016/j.molcel.2022.03.022.
[28] Liu K, Li H, Wang F, Su Y. Ferroptosis: mechanisms and advances in ocular diseases. Molecular and Cellular Biochemistry. 2023; 478: 2081–2095. https://doi.org/10.1007/s11010-022-04644-5.
[29] Li Y, Sun M, Cao F, Chen Y, Zhang L, Li H, *et al*. The Ferroptosis Inhibitor Liproxstatin-1 Ameliorates LPS-Induced Cognitive Impairment in Mice. Nutrients. 2022; 14: 4599. https://doi.org/10.3390/nu14214599.
[30] Wang H, Liu D, Zheng B, Yang Y, Qiao Y, Li S, *et al*. Emerging Role of Ferroptosis in Diabetic Kidney Disease: Molecular Mechanisms and Therapeutic Opportunities. International Journal of Biological Sciences. 2023; 19: 2678–2694. https://doi.org/10.7150/ijbs.81892.
[31] Lu Q, Yang L, Xiao JJ, Liu Q, Ni L, Hu JW, *et al*. Empagliflozin attenuates the renal tubular ferroptosis in diabetic kidney disease through AMPK/NRF2 pathway. Free Radical Biology & Medicine. 2023; 195: 89–102. https://doi.org/10.1016/j.freeradbiomed.2022.12.088.
[32] Li J, Li L, Zhang Z, Chen P, Shu H, Yang C, *et al*. Ferroptosis: an important player in the inflammatory response in diabetic nephropathy. Frontiers in Immunology. 2023; 14: 1294317. https://doi.org/10.3389/fimmu.2023.1294317.
[33] Park JE, Lee H, Kim SY, Lim Y. *Lespedeza bicolor* Extract Ameliorated Renal Inflammation by Regulation of NLRP3 Inflammasome-Associated Hyperinflammation in Type 2 Diabetic Mice. Antioxidants (Basel, Switzerland). 2020; 9: 148. https://doi.org/10.3390/antiox9020148.
[34] Deng Q, Zhu Y, Zhang M, Fei A, Liang J, Zheng J, *et al*. Ferroptosis as a potential new therapeutic target for diabetes and its complications. Endocrine Connections. 2023; 12: e220419. https://doi.org/10.1530/EC-22-0419.
[35] Tang X, Li X, Zhang D, Han W. Astragaloside-IV alleviates high glucose-induced ferroptosis in retinal pigment epithelial cells by disrupting the expression of miR-138-5p/Sirt1/Nrf2. Bioengineered. 2022; 13: 8240–8254. https://doi.org/10.1080/21655979.2022.2049471.
[36] Huang J, Chen G, Wang J, Liu S, Su J. Platycodin D regulates high glucose-induced ferroptosis of HK-2 cells through glutathione peroxidase 4 (GPX4). Bioengineered. 2022; 13: 6627–6637. https://doi.org/10.1080/21655979.2022.2045834.
[37] Sarkar S, Poon CC, Mirzaei R, Rawji KS, Hader W, Bose P, *et al*. Microglia induces Gas1 expression in human brain tumor-initiating cells to reduce tumorigenecity. Scientific Reports. 2018; 8: 15286. https://doi.org/10.1038/s41598-018-33306-0.
[38] Li W, Wang P, Zhang Z, Wang W, Liu Y, Qi Q. MiR-184 Regulates Proliferation in Nucleus Pulposus Cells by Targeting GAS1. World Neurosurgery. 2017; 97: 710–715.e1. https://doi.org/10.1016/j.wneu.2016.01.024.
[39] Luna-Antonio BI, Rodríguez-Muñoz R, Namorado-Tonix C, Pérez-López A, Sanchez EI, Vergara P, *et al*. Expression of growth arrest specific 1 (Gas1) in the distal tubules and collecting ducts in normal kidney and in the early stages of diabetic nephropathy. Journal of Molecular Histology. 2022; 53: 925–946. https://doi.org/10.1007/s10735-022-10104-7.
[40] Baird L, Yamamoto M. The Molecular Mechanisms Regulating the KEAP1-NRF2 Pathway. Molecular and Cellular Biology. 2020; 40: e00099–20. https://doi.org/10.1128/MCB.00099-20.
[41] Yang J, Hua Z, Zheng Z, Ma X, Zhu L, Li Y. Acteoside inhibits high glucose-induced oxidative stress injury in RPE cells and the outer retina through the Keap1/Nrf2/ARE pathway. Experimental Eye Research. 2023; 232: 109496. https://doi.org/10.1016/j.exer.2023.109496.